Interferometric measurements of dynamic polarizabilities for metal atoms using electrically exploding wires in vacuum

G. S. Sarkisov*
Ktech Corporation, 1300 Eubank Boulevard, Albuquerque, New Mexico 87123, USA

I. L. Beigman and V. P. Shevelko
P.N. Lebedev Physical Institute, Moscow 119991, Russia

K. W. Struve
Sandia National Laboratories, Albuquerque, New Mexico 87185, USA
(Received 23 January 2006; published 5 April 2006)

Measurements within 10% accuracy of the dynamic dipole polarizabilities $\alpha(\lambda)$ for five nonrefractory metal atoms (Mg, Ag, Al, Cu, and Au) at laser wavelengths of $\lambda=532$ and 1064 nm are presented using electrical explosion of thin wires in vacuum and a novel laser probing integrated-phase technique. The technique is based on single-wavelength interferometry and does not require axial symmetry of the tested object. Theoretical prediction of $\alpha(\lambda)$ for wavelengths $\lambda=355$, 532, and 1064 nm, as well as the static dipole polarizabilities α_{st}, are also presented. An agreement within 20% was obtained between calculated data, recommended static polarizabilities α_{st}, and the measured dynamic polarizabilities α(532 nm) and α(1064 nm).

DOI: 10.1103/PhysRevA.73.042501 PACS number(s): 32.10.Dk, 52.70.Kz, 52.80.Qj

I. INTRODUCTION

Static and dynamic dipole polarizabilities of atoms and ions are required to obtain many atomic characteristics such as induced dipole moments, oscillator strengths, energy-level shifts (Stark effect), Van der Waals constants, and other characteristics related to the interaction of atomic systems with external electric fields (see Refs. [1,2]). Experimental data even for static polarizabilities are very limited, especially for metal atoms, while dynamic polarizabilities are mainly taken from theoretical calculations (see Refs. [3–5]).

There are two main experimental techniques to measure atomic polarizability: a bulk diagnostic (dielectric constant, refractive index, Rayleigh scattering, Kerr effect), and a beam diagnostic (electric deflection, E-H balance, beam-resonance, light force, atomic interferometry) [3]. The main problem in application of laser interferometry to measure the dynamic atomic polarizability of metallic vapor/gas is determination of the atomic density along the probing path length. To solve this problem it was proposed in Ref. [6] to use laser interferometry and x-ray shadowgraphy simultaneously. Interferometry gives information about the refraction coefficient of a gaseous wire column, while x-ray shadowgraphy provides information about spatial distribution of metal atoms. The main problems with this technique are related to pre-ionization of the gas column by the x-ray probing radiation, a need for axial symmetry to allow reconstruction of the local atomic density, and the high cost of an experiment (because a high-current accelerator ~0.5 MA–100 ns should be used). Interferograms of exploding uncoated and coated 25 μm Ag wires demonstrated in Ref. [6]. show a comparable influence of free and bound electron refractivity. In this case, it is necessary to use two-wavelength interferometry to eliminate the influence of free electrons [7].

In the present work, an application of a novel integrated-phase technique (IPh-technique) for measurement of dynamic atomic polarizability at 532 and 1064 nm for five nonrefractory metals (Al, Mg, Cu, Ag, and Au) is demonstrated using electrical explosion of thin wires in vacuum. The IPh technique is based on the equality of the radial integral of the interference phase shift with the initial linear atomic density of a metal wire. This technique can be applied only for totally vaporized metal wires in vacuum and does not require axial symmetry of the tested object. Theoretical predictions of the static α_{st} and dynamic dipole polarizabilities $\alpha(\lambda)$ of Mg, Ag, Al, Cu, and Au atoms at $\lambda=355$, 532, and 1064 nm are also presented. Our predictions agree within 20% with recommended static polarizabilities α_{st} and experimental dynamic polarizabilities α(532 nm) and α(1064 nm).

II. EXPERIMENTAL SETUP

The experimental setup is presented in Fig. 1. A 100-kV Maxwell 40151-B (positive output) pulse generator with a

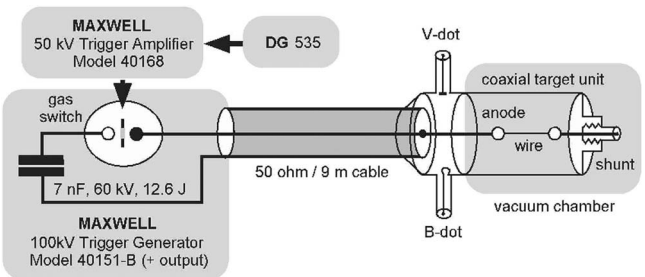

FIG. 1. Electrical circuit diagram.

*Email address: gssarki@sandia.gov

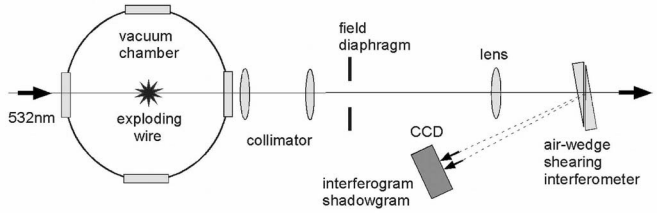

FIG. 2. Optical setup.

7-nF capacitor bank with a charging voltage of 60 kV and stored energy of 12.6 J provided the electrical pulse to drive the wire explosions. A 50-kV Maxwell 40168 trigger amplifier triggered the gas switch of the pulse generator. A digital delay generator (Stanford DG-535) was used to synchronize the trigger amplifier with the diagnostics. Pulse generator jitter was ~2 ns. A 9-m 50-Ω coaxial cable (RG 220/U) delivered the electrical pulse from the generator to the wire. Thin 10–40 μm diameter and 20 mm length wires (Mg, Ag, Al, Cu, and Au) were placed across the cathode-anode gap forming the center conductor of the coaxial target unit. The assembly was evacuated to a pressure of $\sim 10^{-4}$–10^{-5} torr to prevent gas breakdown.

The experiment could operate in either a fast or slow mode. In the fast mode, the current rate was ~150 A/ns into a short circuit (~3 kA maximum) and the voltage rate was ~12 kV/ns into an open circuit (~120 kV maximum). The slow-mode current rate was ~22 A/ns into a short circuit (~2 kA maximum) and voltage rate was ~1 kV/ns into an open circuit (~80 kV maximum). The ~100-ns oscillation period of the current was related to the impedance mismatch presented by the coaxial target unit. However, the mismatch was not relevant since energy deposition and wire explosion occurred during the first 50 ns.

The downstream current through the wire was measured with a 2-GHz bandwidth, 0.1-Ω coaxial shunt resistor. The anode-ground voltage was measured with a capacitive divider with an inductive coil measuring total upstream current. These electrical diagnostics provided upstream and downstream current, voltage, load resistance, and energy deposition into the wire core throughout the wire explosion. A silicon *p-i-n* diode with 1-ns rise time (Thorlabs DET210) monitored light emission power from the exploding wire. A short pulse laser (Ekspla SL-312 with 120 mJ at 532 nm with 150 ps pulse duration) produced shadowgraphy and interferometric images of the exploding wire. All electrical waveforms were captured by a 4-channel, 1 GHz digital oscilloscope (Tektronix TDS 684C, 1 GHz, 5 GS/s). Images were recorded with a high-resolution CCD camera (1500 $\times$ 1000, 12 bit).

Figure 2 shows the optical setup based on a shearing air-wedge interferometer first proposed in [8]. The shearing interferogram and shadowgram images resulted from ~4% internal reflections from two slightly tilted glass air wedges pressed together. The direction and period of the interference lines, as well as the beam overlap, was adjusted by changing the air-wedge angle and position of the interferometer with respect to the focus of the imaging lens [8].

III. MEASUREMENT TECHNIQUE

A. Basic method

During fast nanosecond electrical explosion of thin metal wires in vacuum, the wire material can be totally vaporized and expanded in a radial direction. Wire explosion is accompanied by generation of a low-density, high-temperature plasma shell, voltage breakdown, and switching of the current from the core to a fast expanding (~100 km/s) corona [9]. After breakdown, the wire core expands radially with a velocity close to the speed of sound and adiabatically cools [9]. Because vaporized material expands in the radial direction, the linear density of the expanding gas equals the linear density of the atoms of the initial wire. If the deposited energy is not enough for total vaporization (because breakdown happens during the liquid state), the wire expands mainly in the form of liquid microdrops of submicrometer size [10]. More detail of exploding wire physics can be found in the reviews [11,12]. The latest results of nanosecond explosions of thin Al wires in vacuum combined with careful magnetohydrodynamic (MHD) simulation are presented in [9].

B. Interferometric sensitivity to the detection of the expanding wire mass

To clarify the sensitivity of the interferometric method for detecting the expanding wire mass, we calculated the interference phase shift of laser light of 532 nm wavelength after propagation through a gas cylinder (see Fig. 3) using a Gaussian-like radial distribution of atoms (which is typical for exploding wire experiments in vacuum),

$$N_A(r) = N_0[1 - (r/r_0)^2]^3, \tag{1}$$

where N_0 is the peak atomic number density and r_0 is the boundary radius of the distribution.

As a sensitivity threshold of the interferometry, we consider a phase shift of $2\pi/20$ (0.05 lines). Initial distributions of the gas density, corresponding to the different moments of expansion for 20 μm diameter Al wires, are presented in Fig. 4(a). For all atomic density distributions, the linear density was constant, that is, 1.9×10^{17} cm^{-1}, and equal to the linear density of 20 μm diameter Al wire. Simulation results using the dynamic polarizability $\alpha(532\text{ nm}) = 10.8\times10^{-24}$ cm^3 (10.8 Å^3) are presented in Fig. 4(b). For 20-μm Al wire that has expanded to a diameter less than 3 mm, at least 98% of the wire mass is inside the sensitivity region of interferometry.

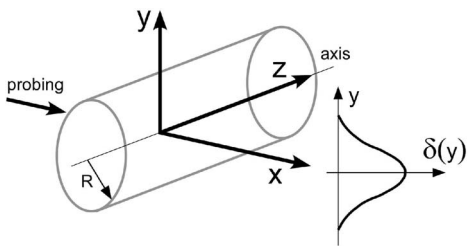

FIG. 3. Probing diagram.

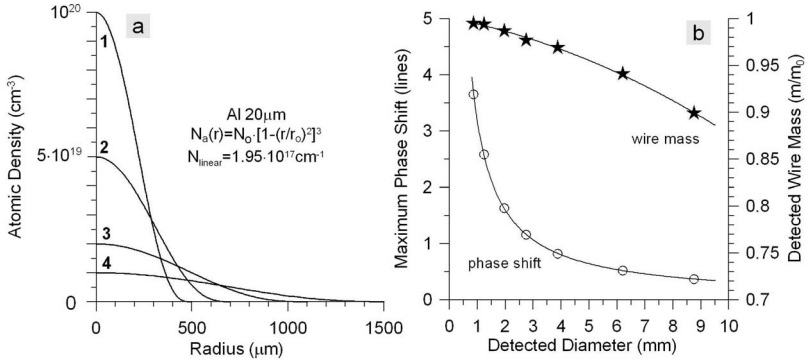

FIG. 4. (a) Radial distributions of atomic density for a 20 μm diameter Al wire at 4 times. (b) Reconstruction of the axial phase shift and detectable wire mass vs detectable wire diameter.

C. Reconstruction of dynamic polarizability using the integrated-phase technique

The integrated-phase technique (IPh-technique) is based on the assumption of equality of the initial linear density of the wire and the radially integrated atomic density inferred from the interferogram. For the gas state of an expanding metal wire core, the interference phase shift can be written as

$$\delta_A(y) = \frac{2\pi}{\lambda}\alpha(\lambda)\int_L N_A dx, \tag{2}$$

where δ_A is the phase shift, N_A is the atomic density, $\alpha(\lambda)$ is the dynamic polarizability, λ is the probe laser wavelength, L is the path length, and x and y are the coordinates along and perpendicular to the laser direction.

Because the initial wire diameter is known, one can calculate the linear density of atoms N_{lin}. Assuming that all of the totally vaporized exploded wire material stays inside the sensitive threshold of the interferometer (see Sec. III B), one can write N_{lin} as

$$N_{\mathrm{lin}} = \int\int N_A dxdy = \frac{\lambda}{2\pi\alpha(\lambda)}\int_Y \delta_A(y)dy, \tag{3}$$

where Y is the length of the disturbance of the phase shift in the radial direction.

Because the wires expand radially, the direction of the phase integration y is perpendicular to the wire axis (see Fig. 3). Therefore, the average dynamic dipole polarizability can be extracted from the linear density of the wire and the integral of the phase shift,

$$\alpha(\lambda) = \frac{\lambda/2\pi}{N_{\mathrm{lin}}}\int_Y \delta_A(y)dy. \tag{4}$$

Note that the main assumptions for application of the IPh-technique for measurement of dynamic polarizability are (i) the wire is totally vaporized, (ii) free-electron refractivity is negligible, and (iii) the exploded wire material stays within the sensitive region of the interferometer. In this approach, axial symmetry of the tested object is not required. If conditions (i)–(iii) are not exactly satisfied, the IPh-technique gives a low estimate of the dynamic dipole polarizability at the probing frequency.

For totally ionized plasma, the contribution of the bound electrons is negligible, and the interferometric phase shift δ_e depends only on the free-electron density n_e,

$$\delta_e(y) = -4.49\times10^{-14}\lambda\int_L n_e dx, \tag{5}$$

where n_e has units cm^{-3}.

Thus, for a totally ionized plasma, the IPh-technique gives the linear density of the free electrons in cm^{-1} as

$$n_{\mathrm{lin}} = -2.23\times10^{13}\lambda^{-1}\int \delta_e(y)dy. \tag{6}$$

To get the absolute number of atoms [Eq. (3)] or electrons [Eq. (6)], it is necessary to do two-dimensional integration of the phase shift $\delta(y,z)$. No axial symmetry is required. But if electronic and atomic refractivity are comparable, it is necessary to use two-wavelength interferometry for splitting electronic and atomic contributions to the total phase shift [7].

D. Estimation of experimental accuracy

According to Eq. (4), there are two sources of error for reconstruction of the average dynamic polarizability: (i) reconstruction of the initial linear density of the wire, and (ii) reconstruction of the interference phase-shift integral. The resulting relative error in the reconstructed dynamic polarizability is a sum of the relative errors in the determination of the wire mass and phase-shift integral.

In our experiments, we use wires from the California Fine Wire Company[13] (CFW). CFW declares the wire diameter tolerances to be within 0.00015 in. ($\sim$0.6 μm). It means that the 20.3 μm wires we used in our experiments have a standard deviation of $\pm$0.3 μm. This diameter uncertainty gives a relative error for the wire mass of $\pm$3%. Furthermore, an increase in the diameter of the tested wire results in a decrease of the mass error.

Relative error in reconstruction of the radial integral of the interference phase shift depends on the experimental conditions, namely on the maximum phase shift and the number of resolvable points in the radial direction of the phase disturbance. Accurate treatment of the interferogram taking into account the initial nondisturbing distribution of interference lines gives a phase-shift reconstruction accuracy of $\sim 2\pi/20$ [see Fig. (5c)]. For a Gaussian distribution of the radial phase shift with maximum two to three lines, an estimate of the accuracy of phase-shift integration is $\sim$5–7%. So, the total accuracy of the reconstruction of the dynamic polarizability using the IPh-technique can be estimated as $\pm$10%.

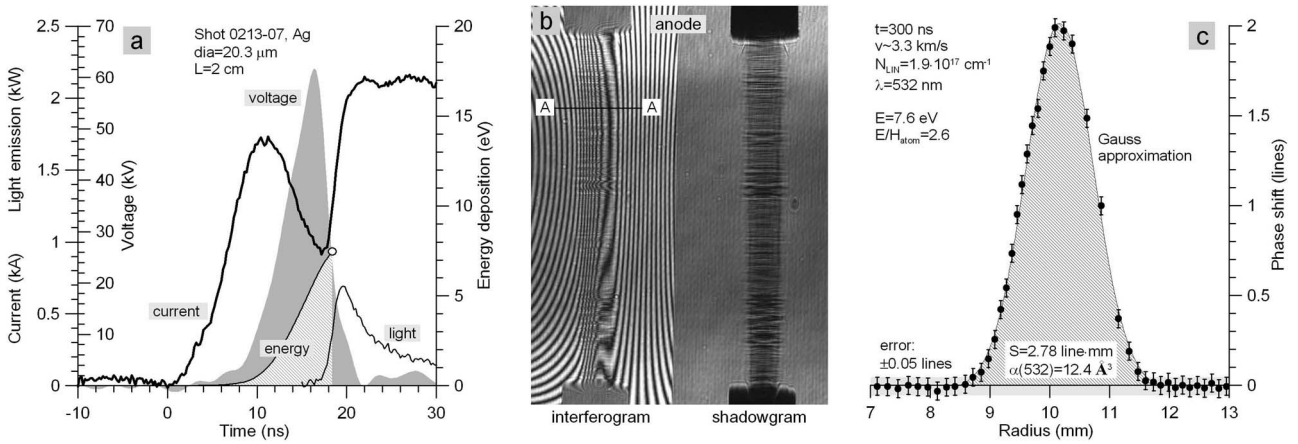

FIG. 5. (a) Current, voltage, light emission, and energy deposition waveforms for exploding 20.3 μm Ag wire; (b) interferogram and shadowgram of the same wire at 300 ns after breakdown; (c) reconstruction of the interference phase shift along the radial cross section A-A.

IV. EXPERIMENTAL RESULTS

Figure 5 demonstrates the data reconstruction procedure for a fast-exploding Ag wire. Figure 5(a) shows the current, voltage, light emission, and energy deposition waveforms for a fast exploding 20.3 μm diameter, 2 cm long Ag wire in vacuum. The voltage rises to ~62 kV in ~16 ns and collapses to almost zero during the next 5 ns. The deposited energy into the wire core, which is the time integral of the electrical power up to the time when the cathode-anode resistance drops two times from its maximum value, was ~7.6 eV/at. This value is 2.6 times the atomization enthalpy for Ag, which is enough for total vaporization. The voltage collapse is related to breakdown of the metal vapor surrounding the wire and rapid switching of the current from the wire core to the fast-expanding plasma shell [9]. After breakdown, the wire expands with a velocity of ~3.3 km/s.

Figure 5(b) shows a complementary interferogram and shadowgram of the exploded Ag wire at ~300 ns after breakdown. Note also that the extended wire core has axial stratifications. Reconstruction of the interference phase shift along the cross-section A-A is presented in Fig. 5(c). The plot shows all the digitized maximum and minimum positions of the interference lines along the A-A line. There are 25 digitized experimental points along the radial direction of the phase disturbance. The experimental points are well approximated by the Gauss function. The reconstruction of the dynamic polarizability with the IPh-technique using these data gives a value of 12.4 Å^3±10%.

To get statistically averaged data, we complete five reconstructions along adjacent cross sections of the same interferogram. Figure 6 shows reconstructions of dynamic polarizability at 532 nm for 35 μm diameter Mg wire and 20.3 μm diameter Au and Al. The dynamic polarizability for Mg has an average value of 13.9 Å^3 with a ±5% uncertainty. The dynamic polarizability of Au and Al has average values of 8.3 and 10.7 Å^3, respectively, with ±3% uncertainty. These uncertainties are primarily related to error in the phase integration and axial redistribution of the linear density due to stratification.

Figure 7 shows reconstructed dynamic atomic polarizability at 532 nm for Ag (a), Al (b), Cu (c), and Au (d), 20.3 μm diameter wires versus deposited energy for different probing times. Each point is a statistical average of five shots. In all cases if the deposited energy is less is than 1.5 times the atomization enthalpy, the reconstruction gives a smaller value for dynamic polarization than with a higher deposited energy. This happens because there is not a total vaporization of the metal. In this case, part of the wire masses in the form

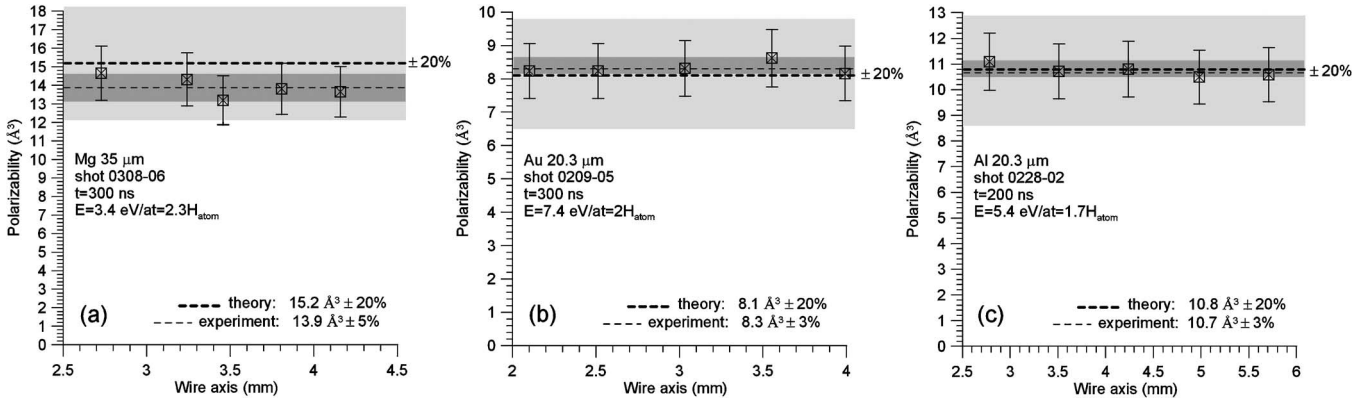

FIG. 6. Reconstruction of dynamic atomic polarizability for the wavelength 532 nm for five different cross sections along the wire length for (a) Mg, (b) Au, and (c) Al.

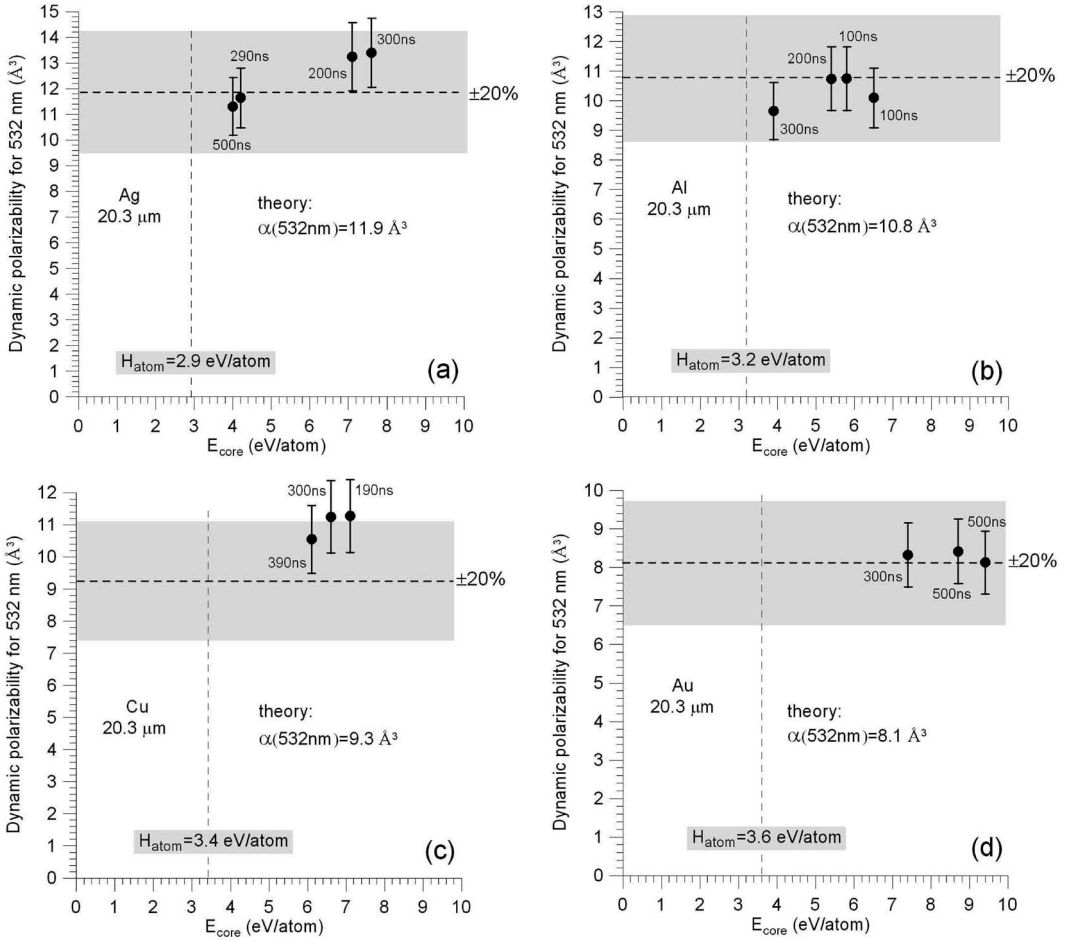

FIG. 7. Dependence of the reconstructed dynamic atomic polarizability at 532 nm vs deposited energy for (a) Ag, (b) Al, (c) Cu, and (d) Au. Each experimental point is statistically averaged and was taken at different times.

of liquid microdrops [10,12] and gives a significantly smaller contribution to the polarizability than the gas components. If the deposited energy is too high and probing time is too early, the expanded metal cylinder can be partially ionized and free electrons may lower the reconstructed value of the polarizability. We can see this effect in Figs. 7(b) and 7(d). In this case, it is reasonable to attribute the maximum value of the reconstructed polarizability in Fig. 7 to the dynamic atomic polarizability of the tested metal; that is, for Ag it is 13.4 $Å^3 \pm 10\%$, for Al it is 10.8 $Å^3 \pm 10\%$, for Cu it is 11.3 $Å^3 \pm 10\%$, and for Au it is 8.3 $Å^3 \pm 10\%$ (see Table I).

Measurements of the dynamic polarizability at a wavelength of 1064 nm were done for exploding Mg and Al wires. For a 35 μm diameter Mg wire, the deposited energy was 3.4 eV/at, which is 2.3 times the atomization enthalpy. Probing time was 400 ns after voltage collapse. The reconstruction of the dynamic polarizability for Mg at 1064 nm gives a value of 12.4 $Å^3 \pm 10\%$. For 25 mm Al wire, the deposited energy was 5.8 eV/at, which is 1.8 times the atomization enthalpy. Probing time was 170 ns after voltage collapse. The reconstruction of the dynamic polarizability for Al at 1064 nm gives a value of 1.8 $Å^3 \pm 10\%$.

TABLE I. Experimentally determined dynamic dipole polarizabilities for Mg, Al, Cu, Ag, and Au atoms at 532 nm (2.33 eV) and 1064 nm (1.16 eV).

Atom	Transition from the ground state to the first dipole allowed state	Transition energy (eV)	Experimental polarizability ($Å^3$) α(532 nm) ±10%	α(1064 nm) ±10%
Mg	$2p^6 3s^2$-$2p^6 3s 3p$	4.35	13.9	12.4
Al	$3s^2 3p$-$3s^2 4s$	3.14	10.8	8.7
Cu	$3d^{10} 4s$-$3d^{10} 4p$	3.81	11.3	
Ag	$4d^{10} 5s$-$4d^{10} 5p$	3.74	13.4	
Au	$5d^{10} 6s$-$5d^{10} 6p$	4.95	8.3	

V. THEORETICAL PREDICTIONS AND COMPARISON WITH EXPERIMENT

In order to interpret the experimental data obtained in the present paper, theoretical predictions of dynamic polarizabilities $\alpha(\lambda)$ were made using the well-known quantum-mechanical formula [14],

$$\alpha_0(\lambda) = a_0^3 4Ry^2 \sum_\gamma \left(\sum_{k\neq o} \frac{f_{ok}^{(\gamma)}}{(\Delta E_{ok}^{(\gamma)})^2 - (\hbar\omega)^2} + \int_{I_\gamma}^{\infty} \frac{df^{(\gamma)}/dE}{E^2 - (\hbar\omega)^2} dE \right), \quad \omega = \frac{2\pi c}{\lambda}, \tag{7}$$

$$\sigma^{(\gamma)} = \pi a_0^2 \frac{4\pi e^2}{\hbar c} \frac{df^{(\gamma)}}{dE/Ry}, \tag{8}$$

where a_0 denotes the Bohr radius, $\hbar$ is the Planck constant, c is the speed of light, e is the electron charge, and λ is the wavelength. Here f and df/dE denote the oscillator strength and oscillator strength density for transitions in discrete spectrum and continuum, respectively, ΔE and I_γ denote transition and binding energies, and $\sigma^{(\gamma)}$ denotes the photoionization cross section. Summation over γ includes transitions of atomic inner-shell electrons. The static polarizability α_{st} is defined by Eqs. (7) and (8) with $\omega=0$.

A. Dynamic polarizability of Mg($2p^6 3s^2$)

In this case, the main contribution to the sum (7) is given by the bound-bound $3s_{1/2}$-$np_{1/2}$ transitions. Contributions from transitions involving $3p^6$ shell and photoionization processes are very small. In calculations, the data for the oscillator strengths $f(3s_{1/2}-np_{1/2})$ with $n\leqslant 6$ and the corresponding transition energies were taken from the astrophysical database by Morton [15]. Calculated dipole polarizabilities for Mg at four different frequencies are given in Table II in comparison with recent calculations made in [16] using the analytical form of the Green function. A contribution of photoionization of $2p$ and $3s$ electrons was estimated using the data of Verner *et al.* [17]. As it is seen, the present calculated data and data from [16] agree to within 10%. Our result for the static polarizability is also in good agreement with calculations [18] ($\alpha_{st}=10.7$ Å^3).

TABLE II. Dipole polarizabilities $\alpha(\lambda)$ of Mg.

Polarizability (Å^3)	Theory [16]	Theory (present)
α(355 nm)	11.3	11.8
α(532 nm)	14.6	15.2
α(1064 nm)	11.3	11.8
α_{st}	10.6	10.9

B. Dynamic polarizability of Al($3s^2 3p$)

This case is the most interesting for calculation among other metal atoms considered here because the ground state consists of two close levels with the total angular moment $j=1/2$ and $3/2$ separated by a small energy interval of about 0.02 eV. The strongest are the $3p$-nd transitions with $n\leqslant 6$ and the transitions $3s^2 3p$-$3s3p^2$ from the inner $3s$ shell. Photoionization of the $3p$ electron gives a 30–50% contribution to the total value of $\alpha(\lambda)$ depending on the frequency λ. Contribution of $3s$-electron photoionization is negligible.

The data for oscillator strengths and transition energies of $3p$-nd transitions with $n\leqslant 6$ were taken form Morton [15], and for photoionization cross section of the $3p$ electron from the tables [17]. Since the data for $3s^2 3p$-$3s3p^2$ transitions are absent in the literature, the corresponding f and ΔE values were calculated in the present work using the FAC code (flexible atomic calculations) described in [19]. Within FAC, the bound-state wave functions are calculated using a fully relativistic configuration-interaction method and the jj-coupling scheme. For the strongest $3s^2 3p$-$3s3p^2$ in Al transitions, we obtained $f(3s^2 3p^2 p_{1/2}$-$3s3p^2\ ^2D_{3/2})=0.685$ with $\Delta E=7.95$ eV, $f(^2P_{3/2}$-$^2D_{3/2})=0.858$ with $\Delta E=7.94$ eV, and $f(^2P_{3/2}$-$^2D_{5/2})=0.356$ with $\Delta E=5.50$ eV.

Calculated $\alpha(\lambda)$ values for Al are given in Table III for three wavelengths in comparison with the static polarizability. Contributions of bound-bound transitions from the ground $3p_{1/2}$ and $3p_{3/2}$ states and the averaged polarizabilities are given in the second, third, and fourth columns, a contribution from $3p$ photoionization and the total $\alpha(\lambda)$ values in the fifth and sixth columns, respectively. The contribution of $3s$-electron photoionization is small. The calculations with configuration interaction [20] and experiment [21] give for j-averaged α_{st} the values of 8.6 and 6.8 Å^3, respectively. An agreement between present calculations and measurements, and recommended data for α_{st}, are within 15%.

TABLE III. Dipole polarizability $\alpha(\lambda)$ of Al.

	Calculated values (Å^3)				
Polarizability	Transitions from $3p_{1/2}$	Transitions from $3p_{3/2}$	j-averaged	$3p$ photoionization	Total, j-averaged
α(355 nm)	2.2	5.8	4.6	2.5	7.1
α(532 nm)	6.9	9.5	8.6	2.1	10.8
α(1064 nm)	4.8	7.1	6.3	2.0	8.3
α_{st}	4.4	6.6	5.9	1.9	7.8

TABLE IV. Dipole polarizability of Cu($3d^{10}4s$).

	Calculated values (Å^3)		
Polarizability	$4s$-np transitions	$3d$ photoionization	Total
α(355 nm)	33.4	0.7	34.1
α(532 nm)	8.6	0.7	9.3
α(1064 nm)	5.9	0.7	6.6
α_{st}	5.4	0.7	6.1

C. Dynamic polarizability of Cu($3d^{10}4s$)

Similar to Mg, for Cu atoms the main contribution to the sum (7) is mainly due to the bound-bound $4s_{1/2}$-$np_{1/2}$ transitions with $n \leqslant 7$, and photoionization of $3d$ electrons. The data for the oscillator strengths and the corresponding transition energies were taken from the database by Morton [15], and a photoionization cross section of $3d$ electrons from Verner *et al.* [17]. The results of calculations of dynamic polarizability for Cu are given in Table IV. The main uncertainity of the calculation is that part of the Cu atoms may be in the $3d^9 4s^2$ state. The polarizability of this state requires specific consideration.

D. Dynamic polarizabilities of Ag($4d^{10}5s$) and Au($5d^{10}6s$)

Gold and silver atoms have an atomic structure similar to Cu, i.e., one s electron outside the closed d^{10} shell. Again, the main contribution of bound-bound transitions is given by s-p transitions with $n \leqslant 7$. Contribution to photoionization by d-electrons is very large. The values of f and ΔE for Ag atoms were taken from Morton [15]. In the case of Au, the values for the resonance $6s_{1/2}$-$6p_{1/2}$ and $6s_{1/2}$-$6p_{1/2}$ transitions were taken from Morton [15], and for the other $6s_{1/2}$-np transitions with $n \leqslant 7$ from calculations [22]. In Ref. [22], the f-values were obtained with a one-electron approximation using core polarization effects. The photoionization cross sections of d-electrons were calculated using the ATOM code described in [23]. The ATOM code calculates the radial wave functions of the optical electrons by solving the radial Schrödinger equation with the effective potential of the atomic core. The results of calculations of dynamic polarizabilities for Ag and Au are presented in Tables V and VI. Similar to Cu, there is an uncertainity in the calculation related to the Ag($4d^9 5s^2$) and Au($5d^9 6s^2$) atoms. The polarizability of this state requires specific consideration.

TABLE V. Dipole polarizabilities $\alpha(\lambda)$ of Ag.

	Calculated values (Å^3)		
Polarizability	$5s$-np transitions	$4d$ photoionization	Total
α(355 nm)	45.4	2.7	48.1
α(532 nm)	9.2	2.7	11.9
α(1064 nm)	6.3	2.6	8.9
α_{st}	5.7	2.6	8.3

TABLE VI. Dipole polarizabilities $\alpha(\lambda)$ of Au.

	Calculated values (Å^3)		
Polarizability	$6s$-np transitions	$5d$ photoionization	Total
α(355 nm)	6.3	4.3	10.6
α(532 nm)	4.0	4.1	8.1
α(1064 nm)	3.3	4.0	7.3
α_{st}	3.1	4.0	7.1

E. Comparison with experiment

Table VII finalizes our experimental and computational data. According to the analysis given in Sec. III D, the experimental accuracy should be ±10%. The source of the calculation error is related mainly to the accuracy of the available values for the oscillator strengths and the photoionization cross sections. In the case of light atoms (Mg, Al), these values are known quite well and the accuracy of the calculated polarizabilities is about 10–20 %, while in the case of heavy atoms (Cu, Ag, and Au) this accuracy is about 30–50 % because of the large uncertainty in the photoionization cross sections. According to Table VII, the agreement between the experimental polarizabilities, the static polarizabilities recommended by the CRC Handbook [5], and the calculated polarizabilities obtained in the present work is within 25%.

VI. CONCLUSIONS

Accurate measurements of the dynamic dipole polarizabilities $\alpha(\lambda)$ within ~10% accuracy (except for Cu) for five nonrefractory metal atoms, Mg, Ag, Al, Cu, and Au, at laser wavelengths $\lambda = 532$ and 1064 nm, were made using electrical explosion of thin wires in vacuum and a novel laser probing integrated-phase technique. The new IPh-technique is based on single-wavelength interferometry and does not require axial symmetry of the tested object. The IPh-technique is based on the assumption of the equality of the initial wire linear density with the density determined from the integral of the radial phase shift taken from the exploded-wire interferogram. The main assumptions of the IP-technique are (i) the wire is totally vaporized; (ii) the expanding metal is in a gaseous state; and (iii) the region of sensitivity of the interferogram includes all of the wire mass. If these assumptions are not true, the IPh-technique gives a low estimate for the dynamic polarizability. This technique can be applied to any metal in the form of thin, 20–30 μm diameter wire. More difficult is vaporization of refractory metals such as tungsten. To insure that the metal is totally vaporized, the deposited energy must be 1.5 to 2 times the atomization enthalpy [10].

Theoretical prediction of dynamic polarizability $\alpha(\lambda)$ for wavelengths $\lambda = 355$, 532, and 1064 nm, as well as static dipole polarizabilities α_{st}, are also presented. An agreement to within 25% was obtained between calculated data, static

TABLE VII. Comparison of calculated theoretical values of dynamic and static dipole polarizabilities with experimental data for five metals (in Å^3). CRC table presents calculation data except for Al.

Atom	CRC static polarizability α_{st}	Calculation (±25%)				Experiment (±10%)	
		α_{st}	α(1064 nm)	α(532 nm)	α(355 nm)	α(1064 nm)	α(532 nm)
Mg	10.6±5%	10.9	11.8	15.2	11.8	12.4	13.9
Al	6.8±5%	7.8	8.3	10.8	7.1	8.7	10.8
Ag	7.2±25%	8.3	8.9	11.9	48.1		13.4
Cu	6.1±25%	6.1	6.6	9.3	34.1		11.3
Au	5.8±25%	7.1	7.3	8.1	10.6		8.3

polarizabilities α_{st}, and experimental dynamic polarizabilities α(532 nm) and α(1064 nm), as presented here.

ACKNOWLEDGMENTS

The authors gratefully acknowledge H. Faretto, A. Oxner, and A. Astanovitskiy for technical assistance in the experiment, and Dr. V.G. Pal'chikov for valuable discussions. Special thanks go to Dr. S. Rosenthal for a careful reading of our paper and useful suggestions. The experimental part of this project has been supported partially by DOE, UNR, Cornell, and SNL grants. Sandia is a multiprogram laboratory operated by Sandia Corporation, a Lockheed Martin Company, for the U.S. Department of Energy's National Nuclear Security Administration under Contract No. DE-AC04-94-AL85000.

[1] N. L. Manakov, V. D. Ovsyannikov, and L. P. Rapoport, Phys. Rep. **141**, 319 (1986).
[2] M. Yu. Amusia, *Atomic Photoeffect* (Plenum, New York, 1994).
[3] K. D. Bonin and M. A. Kadar-Kalen, Int. J. Mod. Phys. B **8**, 3313 (1994).
[4] T. M. Miller and B. Bederson, Adv. At. Mol. Phys. **25**, 37 (1988).
[5] T. M. Miller, *Atomic and Molecular Polarizabilities, in CRC Handbook of Chemistry and Physics*, 87th ed. (CRC, Boca Raton, FL, 2004), Chap. 10, p. 167.
[6] S. A. Pikuz *et al.*, Rev. Sci. Instrum. **72**, 1098 (2001); M. Hu and B. R. Kusse, Phys. Rev. A **66**, 062506 (2002).
[7] F. C. Jahoda and G. A. Sawyer, *Optical Refractivity*, in *Methods of Experimental Physics*, edited by R. H. Lovberg and H. R. Griem (Academic Press, New York, 1971), Vol. 9-B, p. 1.
[8] G. S. Sarkisov, Instrum. Exp. Tech. **39**, 727 (1996).
[9] G. S. Sarkisov *et al.*, Phys. Rev. E **71**, 046404 (2005).
[10] G. S. Sarkisov *et al.*, J. Appl. Phys. **93**, 1674 (2004).
[11] F. D. Bennett, *High-temperature Exploding Wires*, in *Progress in High Temperature Physics and Chemistry*, edited by C. A. Rouse (Pergamon Press, New York, 1968), Vol. 2, Chap. 1, p. 1.
[12] S. V. Lebedev and A. I. Savvatimskii, Sov. Phys. Usp. **27**, 749 (1984).
[13] http://www.calfinewire. com
[14] U. Fano and J. W. Cooper, Rev. Mod. Phys. **40**, 441 (1968).
[15] D. C. Morton, URL: http://www.hia-iha.nrc-cnrc.gc.ca/staff/morton_e.html
[16] V. G. Pal'chikov and V. D. Ovsyannikov, Quantum Electron. **34**, 412 (2004); V. D. Ovsyannikov, V. G. Pal'chikov, H. Katory, and M. Takomoto, *ibid.* **36**, 3 (2006).
[17] D. A. Verner, D. G. Yakovlev, I. M. Band, and M. B. Trzhaskovskaya, At. Data Nucl. Data Tables **55**, 233 (1993).
[18] M. W. J. Bromley and J. Mitroy, Phys. Rev. A **65**, 062505 (2002).
[19] M. F. Gu, Astrophys. J. **582**, 1241 (2003).
[20] C. Lupinetti and A. J. Thakkar, J. Chem. Phys. **122**, 044301 (2005); P. Fuentealba, Chem. Phys. Lett. **397**, 459 (2004).
[21] P. Milani, I. Moullet, and W. A. de Heer, Phys. Rev. A **42**, 5150 (1981).
[22] B. N. Chichkov and V. P. Shevelko, Phys. Scr. **23**, 1055 (1981).
[23] V. P. Shevelko and L. A. Vainshtein, *Atomic Physics for Hot Plasma* (IOP, Bristol, 1993).